The Astrophysical Journal, 803:63 (9pp), 2015 April 20 doi:10.1088/0004-637X/803/2/63

DISCOVERY OF A FAINT OUTER HALO MILKY WAY STAR CLUSTER IN THE SOUTHERN SKY

Dongwon Kim, Helmut Jerjen, Antonino P. Milone, Dougal Mackey, and Gary S. Da Costa
Research School of Astronomy and Astrophysics, The Australian National University, Mount Stromlo Observatory, via Cotter Road, Weston, ACT 2611, Australia; dongwon.kim@anu.edu.au
Received 2015 January 1; accepted 2015 February 10; published 2015 April 16

ABSTRACT

We report the discovery of a new, low-luminosity star cluster in the outer halo of the Milky Way. High-quality *gr* photometry is presented, from which a color–magnitude diagram is constructed, and estimates of age, [Fe/H], [α/Fe], and distance are derived. The star cluster, which we designate as Kim 2, lies at a heliocentric distance of ~105 kpc. With a half-light radius of ~12.8 pc and ellipticity of $\epsilon \sim 0.12$, it shares the properties of outer halo globular clusters, except for at higher metallicity ([Fe/H] ~ −1.0) and lower luminosity ($M_V \sim -1.5$). These parameters are similar to those for the globular cluster AM 4, which is considered to be associated with the Sagittarius dwarf spheroidal galaxy. We find evidence of dynamical mass segregation and the presence of extra-tidal stars that suggests that Kim 2 is most likely a star cluster. Spectroscopic observations for radial-velocity membership and chemical abundance measurements are needed to further understand the nature of the object.

Key words: Galaxy: formation – Galaxy: halo – galaxies: dwarf – globular clusters: general – Local Group

1. INTRODUCTION

Globular clusters (GCs) in the outer halo of the Milky Way (MW) hold important clues to the formation and structure of their host galaxy. Most of these rare distant GCs exhibit anomalously red horizontal branch morphology at given metal abundance (Lee et al. 1994) and belong to the so-called "young halo" system (Zinn 1993a). Young halo objects are hypothesized to have formed in external dwarf galaxies that were accreted into the Galactic potential well and disrupted by the Galactic tidal force (Searle & Zinn 1978). This scenario has received considerable support by observational results from the MW and M31 (Da Costa & Armandroff 1995; Marín-Franch et al. 2009; Mackey & Gilmore 2004; Mackey et al. 2010). Indeed, the young halo clusters resemble the GCs located in dwarf galaxies associated with the MW in terms of horizontal branch type (Zinn 1993b; Smith et al. 1998; Johnson et al. 1999; Harbeck et al. 2001) and other properties such as luminosity, age, and chemical abundance (Da Costa 2003).

Despite the significant contribution of modern imaging surveys like the Sloan Digital Sky Survey (Ahn et al. 2014) to the discoveries of new MW satellite galaxies (e.g., Willman et al. 2005; Belokurov et al. 2007; Irwin et al. 2007; Walsh et al. 2007) and extended substructures (e.g., Newberg et al. 2003; Grillmair 2009), only a small number of star clusters have been discovered (Koposov et al. 2007; Belokurov et al. 2010; Balbinot et al. 2013; Kim & Jerjen 2015), and these are typically located in the inner halo of the MW. A new distant MW halo object at 145 kpc, by the name of PSO J174.0675-10.8774, or Crater, was recently discovered simultaneously in two independent surveys (Belokurov et al. 2014; Laevens et al. 2014). Although this stellar system shares the structural properties of GCs in the outer halo of the Galaxy, confirming its true nature still requires additional investigation. Other than PSO J174.0675-10.8774, only six known MW GCs are located at galactocentric distances larger than 50 kpc, namely, AM 1, Eridanus, NGC 2419, and Palomar 3, 4, and 14 (see Table 1). The *Hubble Space Telescope* (*HST*) Advanced Camera for Survey photometry of the Galactic GCs (Sarajedini et al. 2007; Dotter et al. 2011) has confirmed that all of the outer halo GCs except for NGC 2419 have a red horizontal branch and young ages relative to the inner halo GCs (Dotter et al. 2010).

In this paper, we report the discovery of a distant globular cluster in the constellation of Indus. This object was first detected in our ongoing southern sky blind survey with the Dark Energy Camera (DECam) at the 4 m Blanco Telescope at Cerro Tololo Inter-American Observatory (CTIO) and confirmed with deep GMOS-S images at the 8.1 m Gemini–South telescope on Cerro Pachõn, Chile (Sections 2 and 3). The new star cluster, which we designate as Kim 2, is at a distance $D_\odot \sim 105$ kpc and has a low luminosity of only $M_V \sim -1.5$ mag and a metallicity of [Fe/H] ≈ −1.0, slightly higher than the other young halo clusters (Section 4). In Section 5 we discuss the implication of these properties, present evidence for mass segregation in the cluster, and discuss its possible origin.

2. DISCOVERY

As part of the Stromlo Milky Way Satellite Survey[1] we collected imaging data for ~500 deg^2 with the DECam at the 4 m Blanco Telescope at CTIO over three photometric nights from 2014 July 17 to 19. DECam is an array of 62 2 k × 4 k CCD detectors with a 2.2 deg^2 field of view (FOV) and a pixel scale of 0.″27 (unbinned). We obtained a series of 3 × 40 s dithered exposures in the *g* and *r* bands under photometric conditions. The average seeing was 1.″0 for both filters each night. The stacked images were reduced via the DECam community pipeline (Valdes et al. 2014). We used WeightWatcher (Marmo & Bertin 2008) for weight map combination and SExtractor (Bertin & Arnouts 1996) for source detection and photometry. Sources were morphologically classified as stellar or non-stellar objects. For the photometric calibration, we regularly observed Stripe[2] 82 of the Sloan Digital Sky Survey throughout the three nights with 50 s single exposures in each band. To determine zero points and color terms, we matched our instrumental magnitudes with the Stripe 82 stellar

[1] http://mso.anu.edu.au/~jerjen/SMS_Survey.html
[2] http://cas.sdss.org/stripe82/en/

Table 1
Properties of the Seven Most Distant Galactic GCs Known

Parameter	AM 1	Pal 3	Pal 4	Pal 14	Eridanus	NGC 2419	PSO J174.0675 −10.8774[a]	Unit
α_{J2000}	03 55 02.3	10 05 31.9	11 29 16.8	16 11 00.6	04 24 44.5	07 38 08.4	11 36 16.2	h:m:s
δ_{J2000}	−49 36 55	+00 04 18	+28 58 25	+14 57 28	−21 11 13	+38 52 57	−10 52 39	°:′:″
l	258.34	240.15	202.31	28.74	218.10	180.37	274.8	deg
b	−48.47	+41.86	+71.80	+42.19	−41.33	+25.24	+47.8	deg
$D_\odot$	123.3	92.5	108.7	76.5	90.1	82.6	145	kpc
D_{gc}	124.6	95.7	111.2	71.6	95.0	89.9	145	kpc
[Fe/H]	−1.70	−1.63	−1.41	−1.62	−1.43	−2.15	−1.9	dex
r_h(Plummer)	15.2	18.0	16.6	28.0	12.4	22.1	22	pc
$M_{tot,V}$	−4.73	−5.69	−6.01	−4.80	−5.13	−9.42	−4.3	mag

Note. From Harris (1996, and 2010 edition), combined with Laevens et al. (2014) for PSO J174.0675-10.8774.
[a] PSO J174.0675-10.8774 is not yet unambiguously confirmed as a globular cluster.

catalog to a depth of ∼23 mag and fit the following equations:

$$g = g_{\rm instr} + zp_g + c_g(g_{\rm instr} - r_{\rm instr}) - k_g X, \quad (1)$$

$$r = r_{\rm instr} + zp_r + c_r(g_{\rm instr} - r_{\rm instr}) - k_r X, \quad (2)$$

where zp_g and zp_r are the zero points, c_g and c_r are the respective color terms, k_g and k_r are the first-order extinctions, and X is the mean airmass.

In the Stripe 82 images we observed right after the Kim 2 field, we found 399 stars with $19 < r < 23$ and $0.0 < g - r < 2.0$ in the identical CCD chip where the cluster was detected. We restricted the calibration to stars fainter than $r = 19$ mag to avoid the saturation limit of our DECam data. We determined the zero points, color terms, and associated uncertainties by bootstrapping with replacements performed 1000 times and using a linear least-squares fit with 3σ clipping rejection. Uncertainties in the zero points were measured 0.013 mag in g and 0.010 in r, whereas uncertainties in the color terms are 0.011 and 0.009, respectively. The most recent extinction values k_g and k_r for CTIO were obtained from the Dark Energy Survey team. We calibrated our DECam photometry of the Kim 2 field using these coefficients and corrected for exposure time differences.

We employ the same detection algorithm as described in Kim & Jerjen (2015) to search the photometry catalog for stellar overdensities. In essence, we apply a photometric filter in color–magnitude space adopting isochrone masks based on the Dartmouth stellar evolution models (Dotter et al. 2008a) to enhance the presence of old and metal-poor stellar populations relative to the MW foreground stars. We then bin the R.A., decl. positions of the stars and convolve the 2D histogram with a Gaussian kernel. The statistical significance of potential overdensities is measured by comparing their signal-to-noise ratios (S/N) on the density map to those of random clustering in the residual Galactic foreground. This process is repeated for different bin sizes and Gaussian kernels by shifting the isochrone masks over a range of distance moduli $(m - M)$ from 16 to 22 mag. We detected the new stellar overdensity with a significance of $\sim 8\sigma$ relative to the Poisson noise of the Galactic foreground stars. This object that we chose to call Kim 2 was found at $21^{\rm h}08^{\rm m}49\overset{\rm s}{.}97$, $-51^{\rm d}09^{\rm m}48\overset{\rm s}{.}6$(J2000) in the constellation of Indus.

Table 2
GMOS Observing Log for the Images Used in the Analysis

Filter	UT Date	Exposure	Seeing	Airmass
g	2014 Sep 20	9 × 292 s	0.″6–0.″9	1.08–1.12
r	2014 Oct 29	9 × 292 s	0.″8–0.″9	1.23–1.42

3. FOLLOW-UP OBSERVATIONS AND DATA REDUCTION

To investigate the nature of Kim 2, deep follow-up observations were obtained with the Gemini Multi-Object Spectrograph in imaging mode at the 8.1 m Gemini–South telescope through director's time (GS-2014B-DD-3) on September 20, 21, 22, and 30 and October 29. Since 2014 June, GMOS-S is equipped with a new array of three 2048 × 4176 pixel^2 Hamamatsu CCDs with a 5.′5 × 5.′5 FOV and a pixel scale of 0.″08 (unbinned). To reduce readout time, we employed 2 × 2 binning, resulting in a plate scale of 0.″16 pixel^{-1}. A series of 17 × 292 s dithered exposures in g' and 19 × 292 in r' band were observed. These g' and r' filters are similar, but not identical, to the g and r filters used by the SDSS. We chose the nine best images in each band for our photometric analysis. A summary of the selected observations is presented in Table 2.

We employed the latest Gemini IRAF package V1.13 (commissioning release)[3] for data reduction. We applied bias and flat-field images provided by the Gemini science archive for standard GMOS baseline calibration to each exposure using the GIREDUCE task. The three CCD frames of each reduced image were then mosaicked into a single frame using the GMOSAIC task. Figure 1 shows a cutout at the center of a deep g'-band image, formed by combining the nine individual mosaicked frames of the passband using the IMCOADD task, in which Kim 2 is visible as a concentration of faint stars.

The photometry of the reduced GMOS images was carried out using the software package *kitchen_sync* presented in Anderson et al. (2008) and modified to work with GMOS-S data. It exploits two distinct methods to measure bright and faint stars. Astrometric and photometric measurements of bright stars have been performed in each mosaicked image, independently, by using the appropriate point-spread function (PSF) model, and later combined. To derive the PSF models,

[3] http://gemini.edu/node/12227

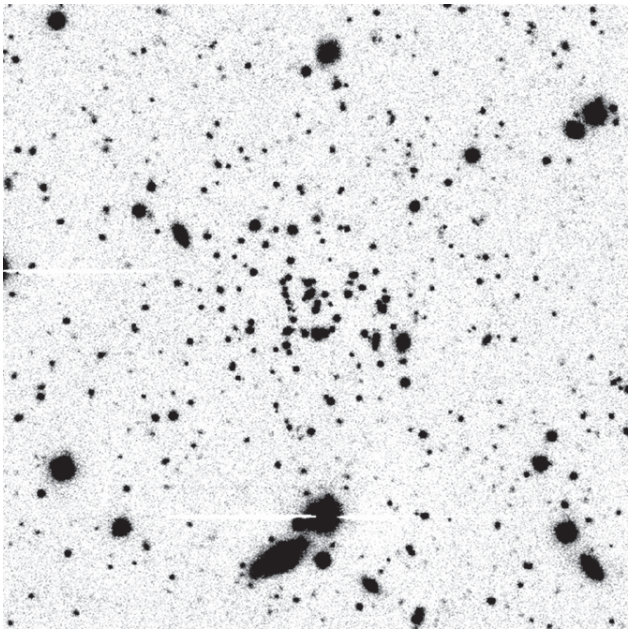

Figure 1. 4 × 4 arcmin^2 GMOS cutout g-band image of Kim 2. The cluster is located at the center of the image. North is up, east is to the left.

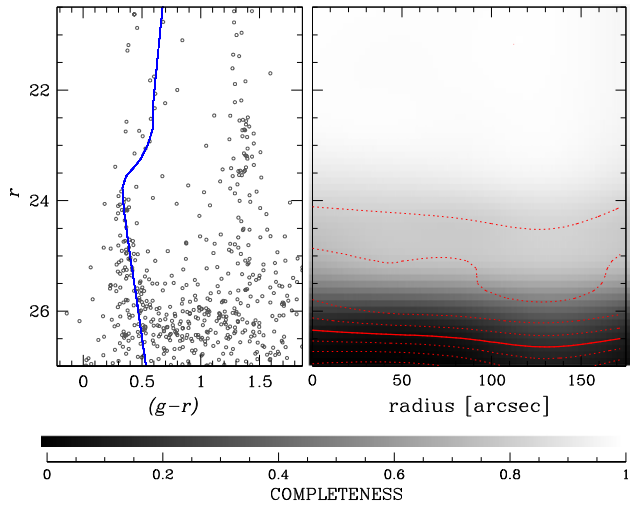

Figure 2. *Left panel*: CMD in instrumental magnitudes. Overplotted on the CMD is the fiducial line along which artificial stars are added. *Right panel*: Completeness contours in the radial distance vs. r magnitude plane. The contour lines correspond to the completeness levels of 90%–20%. The solid contour line marks 50% level.

we adapted to our data the software as described in Anderson & King (2006; see also Bellini et al. 2010). Briefly, we used the most isolated, bright, and non-saturated stars in each image to determine a grid of four empirical PSFs. To account for the spatial variation of the PSF across the FOV, we assumed that to each pixel of the image corresponds a PSF that is a bi-linear weighted interpolation of the closest four PSFs of the grid.

Furthermore, the flux and position can also be determined by fitting for each star simultaneously all the pixels in all the exposures. This approach works better for very faint stars, which cannot be robustly measured in every individual exposure. We refer the reader to the papers by Anderson & King (2006) and Anderson et al. (2008) for further details.

We then conducted the photometric calibration using 65 stars with $22 < r < 25$ and $0.0 < g - r < 2.0$ that we found in the FOV of GMOS. Comparing their instrumental magnitudes to the calibrated magnitudes of our DECam photometry in Section 2, we derived a calibration equation composed of a photometric zero point and a color term from bootstrapping the data 1000 times and performing a least-squares fit with 3σ clipping rejection. Uncertainties in the zero points are 0.022 mag in the g band and 0.023 mag in r. Uncertainties in the color terms are 0.020 and 0.019, respectively.

We performed artificial star tests to determine the completeness level of our photometry. To do this, we used the recipe and the software described in detail by Anderson et al. (2008). Briefly, we first generated an input list of artificial stars and placed along the fiducial line of the MS and the red giant branch (RGB) of Kim 2, which we have derived by hand. The list includes the coordinates of the stars in the reference frame and the magnitudes in g and r bands. Artificial stars have been placed in each image according to the overall cluster distribution as in Milone et al. (2009).

For each star in the input list, the software by Anderson et al. (2008) adds, in each image, a star with appropriate flux and position and measures it by using the same procedure as for real stars. An artificial star is considered to be detected when the input and the output positions differ by less then 0.5 pixels and the input and the output flux by less than 0.75 mag.

The software provides for artificial stars the same diagnostics of the photometric quality as for real stars. We applied the same procedure used for real stars to select a sub-sample of stars with small astrometric errors and well fitted by the PSF. Figure 2 shows the recovery rate of the input stars as a function of the stellar magnitude and the radial distance from the cluster center.

To address the effect of crowding, we measured the completeness as a function of not only the stellar magnitude but also the distance from the cluster center. For the latter, we divided the GMOS field into five concentric annuli, in each of which we measured the completeness in seven magnitude bins, in the interval $-14 < g, r_{\rm instr} < -5$. Interpolating the recovery rate of the input stars at each of these 7 × 5 grid points allows us to estimate the completeness of any star at any position within the cluster, as shown in Figure 2.

4. CANDIDATE PROPERTIES

4.1. Color–Magnitude Diagram

The left panel of Figure 3 shows the R.A.-decl. distribution of all objects classified as point source by our GMOS photometry centered on Kim 2. The middle panel of Figure 3 shows the extinction-corrected color–magnitude diagram (CMD) of all stars located within 1.′3 ($\sim 3r_h$) from the overdensity center. All magnitudes are individually corrected for Galactic reddening by the Schlegel et al. (1998) maps and the extinction coefficients of Schlafly & Finkbeiner (2011). In Table 3, we present our GMOS photometry of all stars brighter than the 50% completeness level, the dotted line in the middle panel of Figure 3. For comparison, the right panel shows the CMD of stars in an equal area between the radii 1.′3 and 1.′8, the majority of which are expected to be MW field stars.

The subgiant branch and the RGB of this loose and faint cluster are almost absent, and no hints of a horizontal branch or red giant clump are visible. The main sequence (MS), however, is well defined down to $r_0 \approx 26.5$, below which our photometry

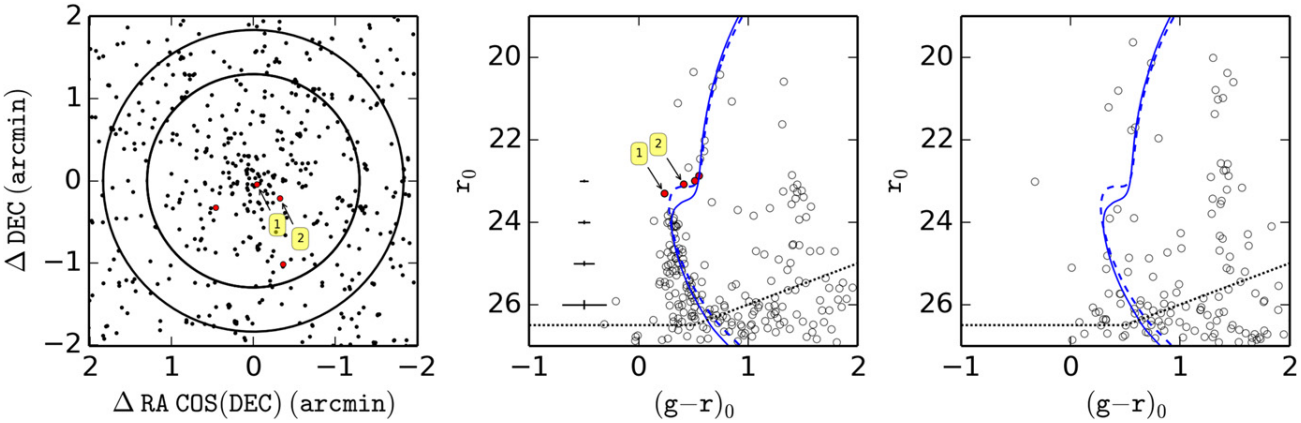

Figure 3. GMOS view of Kim 2. *Left panel*: distribution of all objects classified as stars in a 2′ × 2′ field centered on the cluster. The circles mark a radius of 1.′3 ($\sim 3r_h$) and 1.′8. *Middle panel*: CMD of all stars within the innermost circle marked on the left panel, dominated by the members of the star cluster. *Right panel*: comparison CMD of all stars between the inner and the outer circles, showing the foreground stars. The dotted lines mark the 50% completeness level of our photometry. The two best-fitting Dartmouth isochrones with 11.5 Gyr, [Fe/H] = −1.0, [α/H] = +0.2 (solid line) and with 8.0 Gyr, [Fe/H] = −0.9, [α/H] = +0.4 (dashed line) are overplotted at a distance of 105 and 98 kpc, respectively.

is affected by incompleteness. There are four possible subgiant branch and MS turn-off (MSTO) stars (red dots in Figure 3) consistent with the location of an MS that runs from $r_0 \sim 23.5$ mag down to 26.5 mag. The stars, labeled #1 and #2, have small angular distances from the nominal cluster center (see left panel of Figure 3). This supports the idea that they are cluster members. If true, we would observe a lack of stars between star #1 and the brightest MS stars. Such a gap in the luminosity function (LF) is uncommon but not unheard of, for example, in Segue 3 (see Figure 2 in Fadely et al. 2011). Overplotted on our CMD are two theoretical isochrones from the Dartmouth database. They will be discussed in the next section.

4.2. Age and Metallicity

We estimate the age, metallicity, alpha element to iron abundance, and distance of Kim 2 using the maximum likelihood method described in Frayn & Gilmore (2002), Fadely et al. (2011), and Kim & Jerjen (2015). For the analysis we use all stars within a radius of 1.′3 around Kim 2, the inner circle in the left panel of Figure 3. We calculate the maximum likelihood values $\mathcal{L}_i$, as defined by Equations (1) and (2) in Fadely et al. (2011), over a grid of Dartmouth model isochrones (Dotter et al. 2008a), where i symbolizes the grid points in the multi-dimensional parameter space that covers the age range from 7.0 to 13.5 Gyr, a metallicity range $-2.5 \leqslant$ [Fe/H] $\leqslant -0.5$ dex, $-0.2 \leqslant [\alpha/\mathrm{Fe}] \leqslant +0.4$, and a distance range $19.5 < (m - M) < 20.5$. Grid steps are 0.5 Gyr, 0.1 dex, 0.2 dex, and 0.05 mag, respectively.

In Figure 4, we present the matrix of likelihood values for the sample described above after interpolation and smoothing over two grid points. Depending on the weight given to the two MSTO stars (labeled 1 and 2 in Figure 3), we find two slightly different isochrones that fit the data best (middle panel of Figure 3). If the two stars are given the weights based on their photometric uncertainties, the best-fitting isochrone has an age of 11.5 Gyr, [Fe/H] = −1.0 dex, [α/Fe] = +0.2, and a heliocentric distance of 104.7 kpc ($(m - M) = 20.10$), the solid blue line in Figure 4. However, if we give extra weight to these stars because they are close to the cluster center we derive a younger age of 8.0 Gyr, [Fe/H] = −0.9 dex, [α/Fe] = +0.4, and a distance of 98 kpc ($(m - M) = 19.96$). The probability that goes with this second solution is 0.9% lower than the first solution. In the following we will adopt the parameters of the first solution. In particular, we use a heliocentric distance of 105 kpc for Kim 2 in the calculation of the physical size and absolute magnitude (Section 4.3). The 68%, 95%, and 99% confidence contours are overplotted in Figure 4.

The marginalized uncertainties about this most probable location correspond to an age of $11.5^{+2.0}_{-3.5}$ Gyr, a metallicity of [Fe/H] $= -1.0^{+0.18}_{-0.21}$ dex, and a distance modulus of $(m - M)_0 = 20.10 \pm 0.10$ mag ($D_\odot = 104.7 \pm 4.1$ kpc). For the second solution we get $8.0^{+3.5}_{-2.0}$ Gyr, [Fe/H] $= -0.9^{+0.16}_{-0.19}$ dex, and $(m - M)_0 = 19.96 \pm 0.09$ mag ($D_\odot = 98.2 \pm 4.2$ kpc), respectively.

In the discussion about the age and metallicity of Kim 2 it is important to note that a significant fraction of unresolved MS–MS binaries are common among low-mass star clusters. Some low-luminosity clusters in the Milone et al. (2012) sample like E3 have 50% or more binaries (see their Figure B.4). As we will show in Section 4.3, Kim 2 is among the lowest luminosity (hence lowest mass) star clusters known. If Kim 2 follows the anti-correlation between mass and binary fraction, then it would host a large population of binaries. Unfortunately, our photometry does not allow us to distinguish binaries from single MS stars in the CMD, but we know that binaries are located on the red side of the MS. This means that, due to the presence of many binaries, the MS we observe would be redder than the MS of single stars. Furthermore, binaries of turn-off stars can be located above the turn-off similar to the observed stars we colored in red in the CMD. Hence, if Kim 2 has a high binary fraction, we are likely to overestimate the metallicity by about 0.2–0.4 dex. A detailed study of the binary fraction in Kim 2 shall be the focus of an upcoming study.

Both of our two age/metallicity solutions for Kim 2 are comparable to the observed properties of GCs seen in the Galactic halo. A large ensemble of these objects have been studied in detail with *HST*—see, for example, Figure 13 in Marín-Franch et al. (2009). At [Fe/H] ∼ −1.0 and [α/Fe] ∼ +0.2 ([M/H] ≈ −0.86) we find clusters as young as 0.8 times the age of the oldest systems in the MW; an age of 11.5Gyr would thus be consistent with many other Galactic GCs (albeit lying at smaller galactocentric radii). Moving to the second solution, at

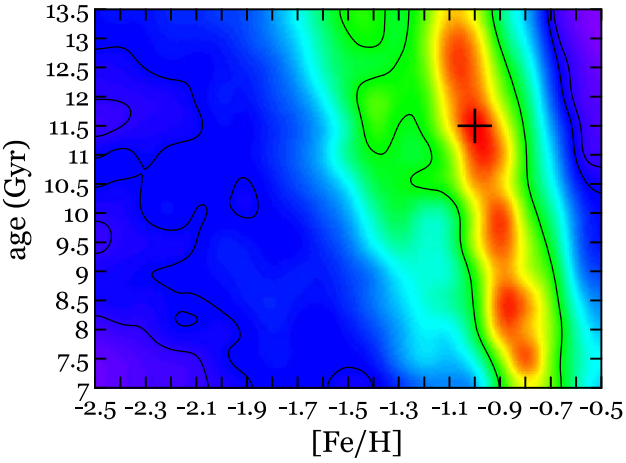

Figure 4. Smoothed maximum likelihood density map in age–metallicity space for all stars within a radius of 1.′3 around Kim 2. Contour lines show the 68%, 95%, and 99% confidence levels. The diagonal flow of the contour lines reflects the age–metallicity degeneracy inherent to such an isochrone fitting procedure. The 1D marginalized parameters around the best fit are age $=11.5^{+2.0}_{-3.5}$ Gyr, [Fe/H] $= -1.0^{+0.18}_{-0.21}$ dex, [α/Fe] = +0.2 dex, and $m - M = 20.10 \pm 0.10$ mag.

[Fe/H] ~ –0.9 or –0.8 and [α/Fe] ~ +0.4 ([M/H] ≈ –0.56), there are clearly somewhat younger clusters than at [M/H] ~ –0.86, but an age of 8.0 Gyr would be certainly on the younger envelope of the observed distribution (this would correspond to a relative age of about 0.6 or so). Note that by this metallicity the age–metallicity relation for Galactic GCs has clearly bifurcated. Clusters on the upper locus are thought to be accreted objects, and Kim 2 would clearly be part of that ensemble. The other point worth mentioning is that [α/Fe] ~ +0.4 at this age and metallicity would be unusually higher than many comparable Galactic GCs. For example, objects with similar ages and metallicities, such as Terzan 7 and Pal 12, have [α/Fe] ~ 0.0. Higher [α/Fe] would suggest that this object came from a relatively massive parent galaxy (perhaps LMC mass or so) where the chemical enrichment proceeded quite quickly, i.e, where the "knee" in the [α/Fe] versus [Fe/H] plot is at comparatively high [Fe/H]. For the older solution [α/Fe] ~ +0.2 and [Fe/H] ~ –1 would seem to be normal compared to other similar Galactic GCs.

4.3. Size, Ellipticity, and Luminosity

The left panel of Figure 5 shows the sky distribution of all GMOS stars in the magnitude range $23.5 < r < 26.5$ and $g < 27.0$ in a 0.°7 × 0.°7 window centered on Kim 2. The solid contours at the center correspond to 3–10σ levels above the background density. We derive an ellipticity $\epsilon = 0.12$ and the position angle $\theta = 35°$ using the fit_bivariate_normal function of the astroML package (VanderPlas et al. 2012). The right panel shows the associated radial profile of the stellar number density, where R_e is the elliptical radius. To estimate the background of field stars, we subtracted from the catalog the stars consistent with the isochrone and counted the remaining stars in the same color–magnitude range, which results in 6.4 stars per square arcminute. The error bars were derived based on Poisson statistics. The best-fit King profile based on the innermost four data points gives a core radius of 0.′28 ± 0.02 or $r_c = 8.5 \pm 0.6$ pc, and a tidal radius of 2.′10 ± 0.02 or $r_t = 64.0 \pm 0.6$ pc adopting the distance modulus of 20.1 mag. We note that the observed radial profile exceeds the King model at radii $R_e > 1.'0$. Such a departure from the King model at radii considerably less than r_t has been already reported for many other GCs and identified as extra-tidal stars that follow a power-law density profile (e.g., Grillmair et al. 1995; Carraro et al. 2007; Carraro 2009). We also estimated a half-light radius by means of the best-fitting Plummer profile, which yields 0.42 ± 0.02 arcmin or $r_h = 12.8 \pm 0.6$ pc (dashed line). Above the King and Plummer profiles, we outline the extra-tidal stars using a power-law profile with slope $\gamma = -2.5$ (dotted line).

We further derived the total magnitude of Kim 2 as follows. We selected Kim 2 stars by means of a photometric filter based on the best-fitting Dartmouth isochrone and taking into account the uncertainties of our photometry. We then built the observed LF of Kim 2 by counting the selected stars within $3r_h$ as a function of magnitude from the saturation level $r_0 = 19.5$ to the 50% completeness limit $r_0 = 26.5$. The observed LF was corrected for incompleteness. We then adopted a normalized theoretical LF based on the Dartmouth model (Dotter et al. 2008a) and scaled it to the observed LF, for which we used two scale factors: (1) the ratio of the integrated number density of the observed LF to the probability density of a normalized theoretical LF between the saturation and the 50% completeness limits and (2) the ratio of the integrated flux of the observed LF to that of the theoretical LF in the same magnitude range. We obtained the total magnitude by integrating the scaled theoretical LF inclusive of the missing flux at r magnitude fainter than the 50% completeness limit. Method 1 yields $M_r = -1.74$ mag and method 2 $M_r = -1.73$ mag. The total V-band luminosity is therefore $M_V = -1.47$ mag ($V - r = 0.264$, adapted from the Dartmouth model for an 11.5 Gyr, [Fe/H] = –1.0 stellar population). Since we included all stars consistent with the isochrone, the calculated value should be considered an upper limit of the true total V-band luminosity, and an exclusion of a single RGB star can change it still by ~0.5 mag. This result suggests that Kim 2 is among the faintest known MW GCs, with a comparable luminosity to Balbinot 1 ($M_V \sim -1.21$; Balbinot et al. 2013), Koposov1 ($M_V \sim -1.35$), and AM 4 ($M_V \sim -1.8$). The only MW star clusters with even lower luminosities are Muñoz 1 ($M_V \sim -0.4$; Muñoz et al. 2012), Koposov2 ($M_V \sim -0.4$; Harris 1996, and 2010 edition), Segue 3 ($M_V \sim 0.0$; Fadely et al. 2011), and Kim1 ($M_V \sim 0.3$; Kim & Jerjen 2015). All derived parameters for Kim 2 are summarized in Table 4.

5. DISCUSSION AND CONCLUSION

We report the discovery of a star cluster, Kim 2, in the outer halo of the MW. This object was first detected in our DECam blind field survey data and confirmed by GMOS follow-up observation. We found the cluster distant (~100 kpc), faint ($M_V \sim -1.4$), younger than the oldest GCs (<11.5 Gyr), and more metal-rich ([Fe/H] ~ –1.0) than any outer halo GC. Its physical size ($r_h \sim 12.8$ pc) is comparable to that of the other outer halo GCs but with an order-of-magnitude difference in terms of luminosity (see Figures 8 and 9 in Mackey & van den Bergh 2005).

5.1. Evidence of Mass Loss

Low-luminosity GCs are expected to be in a mass segregation state as the relaxation time of the clusters is significantly shorter than their respective ages. To estimate the half-mass two-body relaxation time t_{rh} of Kim 2, we used the

Table 3
GMOS Photometry for Stars within $3r_h$ from the Center of Kim 2

α (J2000) (h m s)	δ (J2000) (° ′ ″)	Radial Distance (′)	r (mag)	$(g-r)$ (mag)	α (J2000) (h m s)	δ (J2000) (° ′ ″)	Radial Distance (′)	r (mag)	$(g-r)$ (mag)
21:08:49.81	−51:09:46.66	0.040	24.16	0.37	21:08:46.11	−51:09:52.80	0.608	24.86	1.18
21:08:50.04	−51:09:51.57	0.051	24.42	0.46	21:08:53.28	−51:10:08.69	0.618	23.31	1.52
21:08:49.78	−51:09:51.74	0.060	21.70	1.34	21:08:51.43	−51:09:13.99	0.620	25.80	0.36
21:08:49.68	−51:09:51.33	0.064	23.38	0.27	21:08:47.67	−51:09:18.26	0.621	26.35	0.52
21:08:50.42	−51:09:51.05	0.082	23.83	0.32	21:08:46.14	−51:09:35.97	0.636	25.28	0.29
21:08:49.46	−51:09:50.63	0.087	24.96	0.37	21:08:45.87	−51:09:39.90	0.658	25.83	0.55
21:08:49.50	−51:09:45.45	0.090	26.27	0.52	21:08:46.96	−51:09:20.73	0.662	23.46	1.54
21:08:49.36	−51:09:48.45	0.095	24.18	0.38	21:08:53.62	−51:09:26.57	0.681	21.15	0.88
21:08:49.61	−51:09:43.60	0.100	24.71	0.40	21:08:47.79	−51:09:13.09	0.683	26.09	0.31
21:08:50.46	−51:09:43.76	0.111	25.22	0.42	21:08:48.20	−51:10:26.09	0.683	26.14	0.54
21:08:50.45	−51:09:53.91	0.117	23.97	0.35	21:08:53.07	−51:10:17.52	0.685	25.48	0.50
21:08:49.99	−51:09:41.23	0.123	24.12	0.39	21:08:50.20	−51:09:07.17	0.691	25.85	0.51
21:08:50.48	−51:09:42.44	0.130	25.52	0.61	21:08:50.17	−51:10:30.25	0.695	20.67	1.36
21:08:50.39	−51:09:55.39	0.131	25.50	0.49	21:08:54.46	−51:09:55.98	0.715	25.08	0.32
21:08:50.52	−51:09:41.00	0.154	24.94	0.37	21:08:49.22	−51:09:05.58	0.727	25.98	0.54
21:08:49.12	−51:09:43.51	0.158	23.91	0.30	21:08:54.43	−51:09:31.98	0.752	25.52	0.23
21:08:50.41	−51:09:40.04	0.158	24.81	0.43	21:08:50.76	−51:10:33.49	0.758	25.60	0.47
21:08:50.23	−51:09:58.76	0.174	24.90	0.33	21:08:46.43	−51:09:15.23	0.785	21.19	0.39
21:08:51.21	−51:09:49.31	0.195	25.09	0.45	21:08:49.35	−51:09:00.85	0.802	24.07	0.31
21:08:48.76	−51:09:51.53	0.196	24.36	0.35	21:08:49.65	−51:10:37.71	0.820	20.50	0.77
21:08:51.24	−51:09:50.87	0.203	24.09	0.29	21:08:55.20	−51:09:48.95	0.820	23.64	1.43
21:08:50.36	−51:09:36.70	0.208	24.17	0.33	21:08:50.02	−51:08:58.14	0.841	22.75	0.48
21:08:48.81	−51:09:42.16	0.211	24.74	0.34	21:08:53.89	−51:10:23.19	0.843	25.25	0.37
21:08:48.88	−51:09:58.27	0.234	25.50	1.49	21:08:51.40	−51:10:38.67	0.864	25.90	0.52
21:08:48.46	−51:09:45.11	0.244	25.59	0.51	21:08:51.27	−51:08:57.01	0.884	23.95	1.56
21:08:48.39	−51:09:46.36	0.250	23.92	1.08	21:08:45.25	−51:10:20.17	0.907	25.32	0.31
21:08:49.60	−51:10:04.35	0.269	26.00	0.50	21:08:53.34	−51:09:04.04	0.912	26.30	0.67
21:08:49.67	−51:09:32.71	0.269	25.70	0.50	21:08:44.72	−51:10:12.36	0.914	22.54	0.59
21:08:48.30	−51:09:44.43	0.270	24.17	0.36	21:08:46.21	−51:09:06.23	0.920	25.77	0.49
21:08:51.71	−51:09:52.70	0.282	25.53	0.27	21:08:44.95	−51:10:18.04	0.927	20.80	0.71
21:08:48.41	−51:09:57.73	0.288	24.73	0.36	21:08:47.23	−51:08:58.48	0.939	24.63	1.43
21:08:49.48	−51:10:05.34	0.289	24.04	0.17	21:08:55.76	−51:10:04.42	0.945	24.19	0.35
21:08:51.85	−51:09:46.59	0.297	25.15	0.28	21:08:54.01	−51:10:31.06	0.950	20.43	0.53
21:08:51.62	−51:09:58.41	0.306	25.11	0.30	21:08:44.83	−51:09:16.29	0.969	23.59	0.70
21:08:50.31	−51:09:30.40	0.308	23.70	1.60	21:08:54.60	−51:09:08.32	0.989	26.07	0.39
21:08:50.67	−51:10:06.09	0.312	25.57	0.31	21:08:52.91	−51:10:41.16	0.990	25.63	0.28
21:08:51.88	−51:09:42.67	0.316	24.80	0.30	21:08:55.70	−51:09:21.85	1.003	24.48	0.37
21:08:48.88	−51:10:04.68	0.318	25.27	0.42	21:08:56.36	−51:09:43.54	1.005	25.58	0.92
21:08:50.68	−51:09:30.35	0.324	25.26	0.34	21:08:49.09	−51:08:47.63	1.025	25.96	0.77
21:08:51.56	−51:09:35.91	0.328	25.90	0.43	21:08:56.25	−51:10:08.85	1.040	24.63	0.31
21:08:49.14	−51:09:30.18	0.333	24.97	0.44	21:08:44.24	−51:10:20.47	1.043	23.33	1.35
21:08:47.66	−51:09:47.41	0.363	26.41	0.39	21:08:43.38	−51:10:01.49	1.054	25.58	0.22
21:08:51.13	−51:09:29.50	0.367	22.09	0.63	21:08:56.65	−51:09:59.53	1.063	26.09	0.81
21:08:50.39	−51:10:10.67	0.374	24.61	1.44	21:08:48.50	−51:08:46.22	1.065	25.86	1.00
21:08:49.91	−51:10:11.50	0.382	23.73	1.23	21:08:43.26	−51:10:00.83	1.071	26.09	0.43
21:08:52.32	−51:09:42.66	0.382	26.13	0.82	21:08:55.74	−51:10:24.13	1.082	24.03	0.35
21:08:47.88	−51:10:01.51	0.391	23.16	0.44	21:08:47.64	−51:10:49.72	1.082	23.07	0.54
21:08:52.53	−51:09:53.25	0.409	24.85	0.39	21:08:49.07	−51:08:43.27	1.098	25.99	−0.18
21:08:52.60	−51:09:57.71	0.440	26.42	0.55	21:08:50.56	−51:08:42.41	1.107	24.78	1.10
21:08:52.15	−51:09:31.75	0.443	24.86	0.23	21:08:43.01	−51:10:02.77	1.117	26.45	0.16
21:08:50.66	−51:09:21.20	0.469	25.66	0.47	21:08:44.16	−51:09:09.61	1.119	24.78	1.60
21:08:47.68	−51:09:25.65	0.525	22.35	0.63	21:08:46.02	−51:10:45.91	1.138	23.16	1.48
21:08:46.90	−51:09:33.69	0.542	26.36	0.51	21:08:55.17	−51:10:36.31	1.139	23.78	0.93
21:08:47.50	−51:10:12.08	0.551	22.93	1.43	21:08:56.24	−51:09:14.14	1.140	25.06	0.39
21:08:46.41	−51:09:50.38	0.558	26.21	0.60	21:08:48.42	−51:10:55.57	1.142	26.18	0.72
21:08:47.03	−51:09:29.66	0.558	26.19	0.68	21:08:42.91	−51:09:29.48	1.152	25.07	0.40
21:08:46.65	−51:09:35.71	0.562	26.35	0.54	21:08:45.39	−51:10:42.69	1.152	24.78	1.82
21:08:52.89	−51:10:08.28	0.564	22.95	0.58	21:08:53.20	−51:08:45.94	1.161	25.63	0.50
21:08:52.23	−51:09:22.30	0.564	25.39	0.54	21:08:46.98	−51:08:44.46	1.167	23.50	1.46
21:08:51.70	−51:09:17.53	0.585	25.84	0.61	21:08:43.92	−51:10:29.53	1.168	26.26	0.44
21:08:53.72	−51:09:50.90	0.590	26.29	0.65	21:08:50.94	−51:08:38.12	1.184	24.01	1.50
21:08:50.92	−51:09:14.21	0.592	25.23	1.39	21:08:57.20	−51:09:20.16	1.229	24.74	0.43

Table 3
(Continued)

α (J2000) (h m s)	δ (J2000) (° ′ ″)	Radial Distance (′)	r (mag)	(g − r) (mag)	α (J2000) (h m s)	δ (J2000) (° ′ ″)	Radial Distance (′)	r (mag)	(g − r) (mag)
21:08:53.75	−51:09:49.88	0.593	26.49	0.42	21:08:45.21	−51:08:49.99	1.230	26.37	0.34
21:08:53.24	−51:09:30.70	0.593	24.77	1.69	21:08:42.36	−51:10:06.62	1.230	26.48	0.35
21:08:46.27	−51:09:40.95	0.593	25.36	0.38	21:08:45.70	−51:08:46.41	1.234	24.63	1.50
21:08:46.16	−51:09:53.32	0.603	25.63	0.88	21:08:51.29	−51:08:35.17	1.241	25.50	1.24
21:08:47.36	−51:10:15.60	0.608	25.87	0.31	21:08:43.39	−51:09:05.60	1.256	23.35	1.48

following equation (Spitzer & Hart 1971):

$$t_{rh} = \frac{8.9 \times 10^5 M^{1/2} R_h^{3/2}}{\bar{m} \log_{10}(0.4\, M/\bar{m})}, \quad (3)$$

where M is the mass of a cluster, R_h is the radius containing half mass of the cluster, and $\bar{m}$ is the average mass of the members. Here, we estimated the cluster mass to be $M \sim 600\, M_\odot$ and the average stellar mass to be $\bar{m} \sim 0.3\, M_\odot$ using an initial mass function by Chabrier (2001) and an isochrone by Bressan et al. (2012). We used the half-light radius of 12.8 pc for R_h. Using these numbers gives the relaxation time $t_{rh} \sim 1.1$ Gyr, which is significantly short relative to the estimated age of the cluster(∼11.5 Gyr). This result suggests that Kim 2 should have had sufficient time to undergo dynamical mass segregation. To investigate this possibility, we show in the upper panel of Figure 6 the mass of the stars consistent with the MS of Kim 2 in the magnitude range $23.5 < r_0 < 26.5$ as a function of the distance from the center of the cluster. The stellar mass systematically decreases over the radius. The lower panel shows the normalized cumulative distribution function for three different mass intervals ($0.55 < M/M_\odot < 0.65$, $0.65 < M/M_\odot < 0.75$, and $0.75 < M/M_\odot < 0.85$), corrected for incompleteness. The plots clearly show that more massive MS stars preferentially populate the inner part of the cluster.

Figure 7 shows the distribution of the potential MS stars and contours of 1–6σ levels above the background. Although no tail structure of the extra-tidal stars at radius >1.′0 is noticeable, the outer contours are slightly more elliptical in a rather consistent orientation ($\theta \sim 105$ deg). Similar changes of the orientation angle are observed in the cores of other GCs undergoing tidal disruption (e.g., Pal1, Pal 5, and Pal 14 in Odenkirchen et al. 2001; Niederste-Ostholt et al. 2010; Sollima et al. 2011). Considering the low concentration and luminosity

Table 4
Properties of Kim 2

Parameter	Value	Unit
α_{J2000}	21:08:49.97	h:m:s
δ_{J2000}	−51:09:48.60	° : ′ : ″
l	347.159	deg
b	−42.074	deg
$(m - M)_0$	20.10 ± 0.10	mag
$D_\odot$	104.7 ± 4.1	kpc
D_{gc}	99.4 ± 3.9	kpc
[Fe/H]	$-1.0^{+0.18}_{-0.21}$	dex
[α/Fe]	+0.2	dex
Age	$11.5^{+2.0}_{-3.5}$	Gyr
r_h(Plummer)	12.8 ± 0.6[a]	pc
r_c(King)	8.5 ± 0.6[a]	pc
r_t(King)	64.0 ± 0.6[a]	pc
ϵ	0.12 ± 0.10	⋯
θ	35 ± 5	deg
$M_{tot,V}$	−1.5 ± 0.5	mag

[a] Adopting a distance of 104.7 kpc.

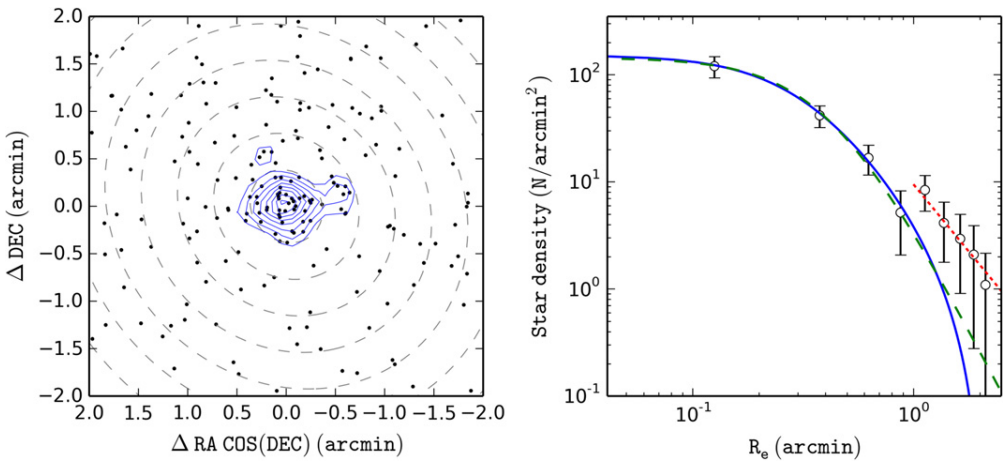

Figure 5. *Left panel*: R.A.–decl. distribution of GMOS stars centered on Kim 2. The dashed ellipses indicate 0.′4 steps in the elliptical radius of ellipcity $\epsilon = 0.12$ and position angle $\theta = 35°$. The solid contours mark the local star density that is 3–10σ above the background density. *Right panel*: radial stellar density profile based on the stellar distribution in the left panel. Open circles represent the star density after subtracting the background contribution. The solid line, dashed line, and dotted line show a King profile with a core radius $r_c = 0.'28$ and tidal radius $r_t = 2.'1$, a Plummer profile with a half-light radius $r_h = 0.'42$, and a power-law profile with a slope $\gamma = -2.5$ for the extra-tidal stars, respectively.

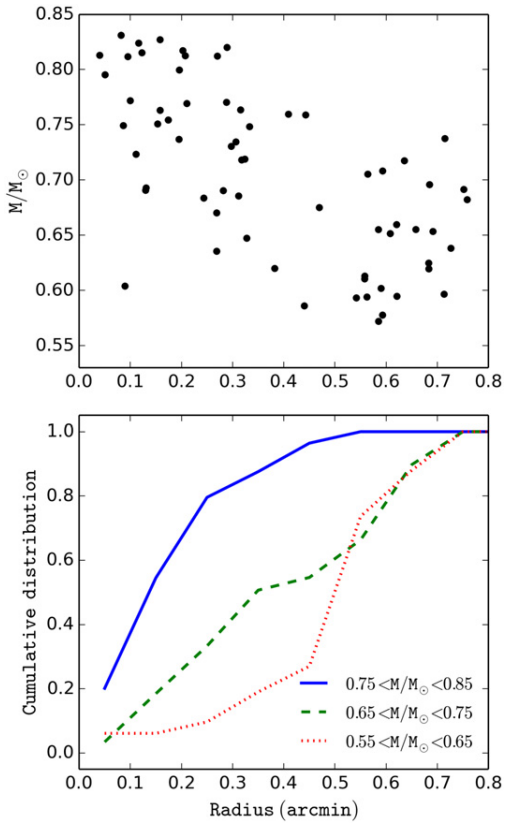

Figure 6. *Upper panel*: stellar mass of all Kim 2 MS stars within $2r_h(\sim 0\farcm8)$ as a function of the distance from the cluster center. *Lower panel*: cumulative distribution function of Kim 2 MS stars for three different mass intervals.

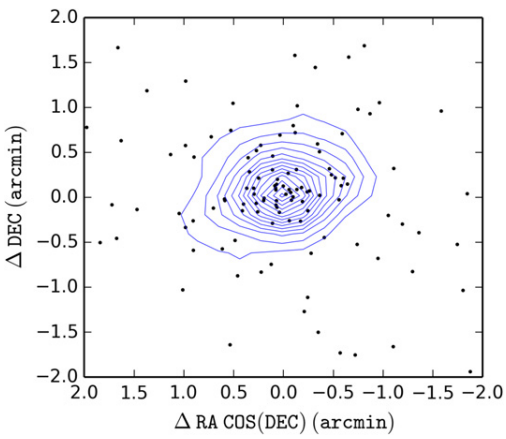

Figure 7. Distribution of stars consistent with Kim 2's MS. Contours mark 1.0–7.5σ levels above the background, with a step size of 0.5σ.

of Kim 2, these stars are likely to be loosely bound around the center.

These results suggest that Kim 2 must have experienced substantial mass loss by relaxation and tidal stripping in order to have reached its current physical and dynamic state. With the consistency between the two-body relaxation time and the observed mass segregation, it seems unlikely that Kim 2 contains any significant amount of dark matter, since otherwise the half-mass radius and the total mass of the system would be much greater than observed, leading to a relaxation time comparable to or even exceeding the Hubble time. Accordingly, dynamical mass segregation would be hardly observed in a dark-matter-dominated stellar system.

5.2. Is Kim 2 Associated with an MW Satellite Galaxy or Stream?

Kim 2 has an unusually low luminosity when compared with the other known outer halo GCs (Table 1). The significant luminosity difference of at least 3 mag and evidence of extra-tidal stars (Section 4.3) strongly suggest that we are seeing an outer halo GC that experienced mass loss due to the MW tidal field, similar to Pal 14 (Sollima et al. 2011). Kim2 and Pal 14 share low star density and evidence of tidal interaction. As suggested by Sollima et al. (2011), an outer halo GC with such low star density is likely to follow an orbit confined to the outer region of the Galactic halo, and/or to have formed in a dwarf galaxy that was later accreted into the Galactic halo. As a consequence, the cluster could have experienced minor tidal disruption and survived until the present epoch.

Kim 2 also shares properties with AM 4 in terms of metallicity, age, and luminosity (Carraro 2009). AM 4 is considered to be associated with the Sagittarius (Sgr) dwarf galaxy. Kim 2 is approximately 25° away from the orbit of the Sgr tidal stream, and the Law & Majewski (2010) model of the Sgr dwarf galaxy embedded in a triaxial MW halo has only a single Sgr Stream particle at a heliocentric distance of 79 kpc within 0.5 deg^2 of Kim 2. This very low particle density and the large line-of-sight distance difference of 26 kpc make it highly unlikely that Kim 2 originates from the Sgr galaxy.

However, there is still the possibility that Kim 2 is not a genuine MW globular cluster, but was formerly associated with another dwarf galaxy, which deposited it into the Galactic halo. In that context, we note that Kim 2 is relatively close to the vast polar structure (VPOS), a thin (20 kpc) plane perpendicular to the MW disk defined by the 11 brightest MW satellite galaxies (Kroupa et al. 2005; Metz et al. 2007, 2009; Kroupa et al. 2010; Keller et al. 2012; Pawlowski et al. 2012). In the region of Kim 2 VPOS is defined by the SMC, LMC, and Carina. GCs and stellar and gaseous streams appear to preferentially align with the VPOS too (Forbes et al. 2009; Pawlowski et al. 2012). The origin of that plane is still a matter of debate. It could be the result of a major galaxy collision that left debris in the form of tidal dwarfs and star clusters along the orbit (Pawlowski et al. 2013). A more detailed analysis of this matter is beyond the scope of this paper due to the small FOV of GMOS and the shallowness of our more extended DECam photometry.

The authors would like to thank Tammy Roderick, Kathy Vivas, and David James for their assistance during the DECam observing run. We also thank the referee for the helpful comments and suggestions, which contributed to improving the quality of the publication. We acknowledge the support of the Australian Research Council (ARC) through Discovery projects DP120100475, DP150100862, and DP1093431 and financial support from the Go8/Germany Joint Research Co-operation Scheme. Based on observations obtained at the Gemini Observatory, processed using the Gemini IRAF package and gemini_python. Gemini Observatory is operated by the Association of Universities for Research in Astronomy, Inc., under a cooperative agreement with the NSF on behalf of the Gemini partnership: the National Science Foundation

(United States), the National Research Council (Canada), CONICYT (Chile), the Australian Research Council (Australia), Ministério da Ciência, Tecnologia e Inovação (Brazil), and Ministerio de Ciencia, Tecnología e Innovación Productiva (Argentina). This project used data obtained with the Dark Energy Camera (DECam), which was constructed by the Dark Energy Survey (DES) collaborating institutions: Argonne National Lab, University of California Santa Cruz, University of Cambridge, Centro de Investigaciones Energeticas, Medioambientales y Tecnologicas-Madrid, University of Chicago, University College London, DES-Brazil consortium, University of Edinburgh, ETH-Zurich, University of Illinois at Urbana-Champaign, Institut de Ciencies de l'Espai, Institut de Fisica d'Altes Energies, Lawrence Berkeley National Lab, Ludwig-Maximilians Universitat, University of Michigan, National Optical Astronomy Observatory, University of Nottingham, Ohio State University, University of Pennsylvania, University of Portsmouth, SLAC National Lab, Stanford University, University of Sussex, and Texas A&M University. Funding for DES, including DECam, has been provided by the U.S. Department of Energy, National Science Foundation, Ministry of Education and Science (Spain), Science and Technology Facilities Council (UK), Higher Education Funding Council (England), National Center for Supercomputing Applications, Kavli Institute for Cosmological Physics, Financiadora de Estudos e Projetos, Fundação Carlos Chagas Filho de Amparo a Pesquisa, Conselho Nacional de Desenvolvimento Científico e Tecnológico and the Ministrio da Ciência e Tecnologia (Brazil), the German Research Foundation-sponsored cluster of excellence "Origin and Structure of the universe," and the DES collaborating institutions.

REFERENCES

Ahn, C. P., Alexandroff, R., Allende Prieto, C., et al. 2014, ApJS, 211, 17
Anderson, J., Bedin, L. R., Piotto, G., Yadav, R. S., & Bellini, A. 2006, A&A, 454, 1029
Anderson, J., Sarajedini, A., Bedin, L. R., et al. 2008, AJ, 135, 2055
Balbinot, E., Santiago, B. X., da Costa, L., et al. 2013, ApJ, 767, 101
Bellini, A., Bedin, L. R., Piotto, G., et al. 2010, AJ, 140, 631
Belokurov, V., Irwin, M. J., Koposov, S. E., et al. 2014, MNRAS, 441, 2124
Belokurov, V., Walker, M. G., Evans, N. W., et al. 2010, ApJL, 712, L103
Belokurov, V., Zucker, D. B., Evans, N. W., et al. 2007, ApJ, 654, 897
Bertin, E., & Arnouts, S. 1996, A&AS, 117, 393
Bressan, A., Marigo, P., Girardi, L., et al. 2012, MNRAS, 427, 127
Carraro, G. 2009, AJ, 137, 3809
Carraro, G., Zinn, R., & Moni Bidin, C. 2007, A&A, 466, 181
Chabrier, G. 2001, ApJ, 554, 1274
Da Costa, G. S., & Armandroff, T. E. 1995, AJ, 109, 2533
Da Costa, G. S. 2003, in ASP Conf. Ser. 296, New Horizons in Globular Cluster Astronomy, ed. G. Piotto, G. Meylan, S. G. Djorgovski, & M. Riello (San Francisco, CA: ASP), 545
Dotter, A., Chaboyer, B., Jevremović, D., et al. 2008, ApJS, 178, 89
Dotter, A., Sarajedini, A., & Anderson, J. 2011, ApJ, 738, 74
Dotter, A., Sarajedini, A., Anderson, J., et al. 2010, ApJ, 708, 698
Fadely, R., Willman, B., Geha, M., et al. 2011, AJ, 142, 88
Frayn, C. M., & Gilmore, G. F. 2002, MNRAS, 337, 445
Forbes, D. A., Kroupa, P., Metz, M., & Spitler, L. 2009, Mercu, 38, 24
Grillmair, C. J. 2009, ApJ, 693, 1118
Grillmair, C. J., Freeman, K. C., Irwin, M., & Quinn, P. J. 1995, AJ, 109, 2553
Harbeck, D., Grebel, E. K., Holtzman, J., et al. 2001, AJ, 122, 3092
Harris, W. E. 1996, AJ, 112, 1487
Irwin, M. J., Belokurov, V., Evans, N. W., et al. 2007, ApJL, 656, L13
Johnson, J. A., Bolte, M., Stetson, P. B., Hesser, J. E., & Somerville, R. S. 1999, ApJ, 527, 199
Keller, S. C., Mackey, D., & da Costa, G. S. 2012, ApJ, 744, 57
Kim, D., & Jerjen, H. 2015, ApJ, 799, 73
Koposov, S., de Jong, J. T. A., Belokurov, V., et al. 2007, ApJ, 669, 337
Kroupa, P., Famaey, B., de Boer, K. S., et al. 2010, A&A, 523, A32
Kroupa, P., Theis, C., & Boily, C. M. 2005, A&A, 431, 517
Laevens, B. P. M., Martin, N. F., Sesar, B., et al. 2014, ApJL, 786, L3
Law, D. R., & Majewski, S. R. 2010, ApJ, 714, 229
Lee, Y.-W., Demarque, P., & Zinn, R. 1994, ApJ, 423, 248
Mackey, A. D., & Gilmore, G. F. 2004, MNRAS, 355, 504
Mackey, A. D., Huxor, A. P., Ferguson, A. M. N., et al. 2010, ApJL, 717, L11
Mackey, A. D., & van den Bergh, S. 2005, MNRAS, 360, 631
Marín-Franch, A., Aparicio, A., Piotto, G., et al. 2009, ApJ, 694, 1498
Marmo, C., & Bertin, E. 2008, adass, 394, 619
Metz, M., Kroupa, P., & Jerjen, H. 2007, MNRAS, 374, 1125
Metz, M., Kroupa, P., & Jerjen, H. 2009, MNRAS, 394, 2223
Milone, A. P., Bedin, L. R., Piotto, G., & Anderson, J. 2009, A&A, 497, 755
Milone, A. P., Piotto, G., Bedin, L. R., et al. 2012, A&A, 540, AA16
Muñoz, R. R., Geha, M., Côté, P., et al. 2012, ApJL, 753, L15
Newberg, H. J., Yanny, B., Grebel, E. K., et al. 2003, ApJL, 596, L191
Niederste-Ostholt, M., Belokurov, V., Evans, N. W., et al. 2010, MNRAS, 408, L66
Odenkirchen, M., Grebel, E. K., Rockosi, C. M., et al. 2001, ApJL, 548, L165
Pawlowski, M. S., Kroupa, P., & Jerjen, H. 2013, MNRAS, 435, 1928
Pawlowski, M. S., Pflamm-Altenburg, J., & Kroupa, P. 2012, MNRAS, 423, 1109
Sarajedini, A., Bedin, L. R., Chaboyer, B., et al. 2007, AJ, 133, 1658
Schlafly, E. F., & Finkbeiner, D. P. 2011, ApJ, 737, 103
Schlegel, D. J., Finkbeiner, D. P., & Davis, M. 1998, ApJ, 500, 525
Searle, L., & Zinn, R. 1978, ApJ, 225, 357
Smith, E. O., Rich, R. M., & Neill, J. D. 1998, AJ, 115, 2369
Sollima, A., Martínez-Delgado, D., Valls-Gabaud, D., & Peñarrubia, J. 2011, ApJ, 726, 47
Spitzer, L., Jr., & Hart, M. H. 1971, ApJ, 164, 399
Valdes, F., Gruendl, R., & DES Project 2014, in ASP Conf. Ser. 485, Astronomical Data Analysis Software and Systems XXIII, ed. N. Manset, & P. Forshay (San Francisco, CA: ASP), 379
VanderPlas, J., Connolly, A., Ivezić, Ž., & Gray, A. 2012, in Conference on Intelligent Data Understanding (CIDU), ed. K. Das, N. V. Chawla, & A. N. Srivastava (Los Alamitos, CA: IEEE), 47
Walsh, S. M., Jerjen, H., & Willman, B. 2007, ApJL, 662, L83
Willman, B., Blanton, M. R., West, A. A., et al. 2005, AJ, 129, 2692
Zinn, R. 1993a, in ASP Conf. Ser. 48, The Globular Cluster-Galaxy Connection, ed. G. H. Smith, & J. P. Brodie (San Francisco, CA: ASP), 38
Zinn, R. 1993b, in ASP Conf. Ser. 48, The Globular Cluster-Galaxy Connection, ed. G. H. Smith, & J. P. Brodie (San Francisco, CA: ASP), 302